Article submitted to: High Power Laser Science and Engineering, 2023 *December 14, 2023*

A simple method for pulse contrast enhancement via self-focusing effect

Zaharit Refaeli[1,2], Gilad Marcus[2], and Yariv Shamir[1]

[1]*Applied Physics Division, Soreq NRC, Yavne, 8180000, Israel*
[2]*Applied Physics Institute, The Hebrew University, The Edmond J. Safra Campus - Givat Ram, 9112001, Jerusalem, Israel*

Abstract
Here we report on a simple-to-implement and cost-effective approach for laser pulse contrast enhancement, based on $\chi^{(3)}$ nonlinear self-focusing effect. An intentionally induced and gently controlled self-focusing in a thin glass, transforms the time dependant intensity into variation in beam divergence. Followed by a spatial discriminating filter, only the strongly focused fraction traverse the setup, at the expense of efficiency. Numerical model, accounting for pulse and material parameters via Gaussian ABCD matrix, provides an estimate for the instantaneous beam waist and transmission efficiency, which enables us to evaluate a resulted contrast enhancement. The estimated contrast enhancement spans between half to 2.5 orders of magnitude, in conjunction with $\sim$ 90% - 25% estimated efficiency, depending on pulse parameters. In a preliminary experiment we demonstrated the effect with 10s μJ sub GW regime with $\sim 40\%$ efficiency and $\geq$ 20 dB contrast improvement.

Keywords: Ultrafast laser, Pulse contrast, Nonlinear optics, Self-focusing

1. Introduction

Since the appearance of high energy short pulse laser systems based on Chirp Pulse Amplifiers (CPA)[1], it became apparent that certain experiments can be hindered by pulse parts that are not confined to its peak vicinity. It is therefore important to define the pulse contrast ratio, i.e., the ratio between the peak intensity and intensities extended towards the pulse pedestals. As a result, high field experiments made pulse contrast a property of vast importance. In that context, the most demanding experiments are those involving the interaction of intense light with solids[2,3], as they start to dissociate into plasma. Typically, solid targets experience coulomb explosion under intensities of above 10^{10} and 10^{13} W/cm^2 [4] for nanosecond (ns) pedestals or picosecond (ps) pre-pulses, correspondingly[5]. Once the plasma becomes over-critical, i.e., plasma density scale length increases, interaction is hindered. Hence, when intensities are on the order of $10^{17} - 10^{21}$ W/cm^2, contrast level must be kept above $\sim 10^7 - 10^{11}$, respectively.

In recent decades, several techniques were developed to clean up pulses, most are based on instantaneous gating mechanisms obtained by nonlinear (NL) processes. Amongst one can list, e.g., Cross-Polarized Wave (XPW)[6], Second-Harmonic Generation (SHG)[7], Optical Parametric Amplification (OPA) and specifically, Optical Parametric Chirped Pulse Amplification (OPCPA)[8–10], Plasma Mirrors (PM)[11,12], Self-Diffraction (SD)[13–15], etc.. Methods such as those mentioned above typically clean up pulses by two to five orders of magnitude, with reported value of even 70 dB improvement[16] . As with most nonlinear processes, the above mentioned cases are associated with significant energy penalty, i.e. efficiencies ranging from tens to a few percent.

An exceptional result was introduced in 2020, with an approach based on a spatial NL plasma lens that was generated by an auxiliary pump beam[17]. While achieving contrast enhancement (CE) of two orders of magnitude, with impressive efficiency of $\sim$80%, such a method entails significant awkwardness, as it necessitates slaving a secondary laser into the process and accurately synchronize it with the main laser.

The approach described in this work is based on a self-induced single-beam effect, which is achieved by simply activating the basic Kerr-lens (KL) effect[18] using peak powers significantly beyond the critical peak power for self focusing ($\sim$4 MW for Gaussian beam in glass). Given thin enough sample (i.e., before the beam collapse occurs inside the bulk material[19]), followed by a succeeding spatial filtration. Since the NL lens constitutes temporal-spatial-temporal mapping, the latter filtration translates to temporal

10.1017/hpl.2023.99

cleaning, as elaborated below. Obviously, such process occur in-line, is self induced and requires no alignment to achieve the effect. Although some similarities to the above-mentioned plasma lens exits, the proposed method is far easier to implement since it is a self-induced process and doesn't require any additional optically synchronized sources, nor unique materials.

Using KL in the context of pulse cleaning was sought after in a work published in 1975, in form of a numerical model that simulated KL mechanism inside a laser oscillator for contrast enhancement[20]. However, since the model was based on blocking the center of the beam, it predicted optimal operation only inside oscillators, whereas for amplifier applications it is expected to introduce low efficiency. Naturally, under much higher energies such process is less attractive. This drawback can, in the present context, be offset by certain variations in the model's scheme, as proposed here. Interestingly, in the recent decade, the spatial beam aspect affected by KL was found to enhance certain laser beam properties. Liu *et-al* have demonstrated spatial cleanup, namely M^2 beam parameter reduction via KL, induced by a short pulse in a multi-mode graded-index fiber[21]. Against most of the CE efforts, intentional reduction of pulse contrast via KL effect was demonstrated in 2019[22] with the purpose of measuring high pulse contrast with a limited diagnostics. The current study follows an alternative path to the latter, that with some further modification, can achieve pulse CE.

In 2021, an experimental study on Kerr lens affect on CE demonstrated the use of multiple plates and a succeeding filter[23]. This study indeed confirmed the validity of the self-focusing approach for CE. The work presented here proposes a complementary approach, providing both thorough numerical model, and a validation with a single stage nonlinear element.

2. Kerr lens approach

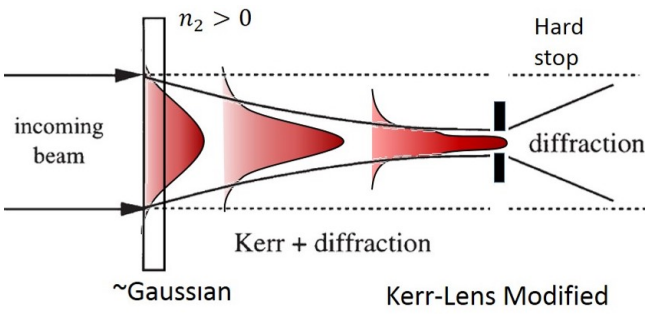

Figure 1. An Illustration showing the spatial shaping of a Gaussian beam affected by the temporal intensity change, which in turn modify the medium.

Here, we propose a method that uses KL to discriminate between different time-varying pulse intensity levels. In a simplified description, the technique is aimed to improve contrast via gently controlled KL excitation in a relatively thin dielectric, i.e. the beam experiences negligible transverse variations while traversing a short path along the dielectric. However, it induces angular convergence, as elaborated below. The method's principle is of translating time varying pulse intensity profile to corresponding variations in its spatial dimensions, that is, beam waist size, and then consecutively applying spatial filtration. The latter spatially modifies parts that traverses the filter, which, in turn, affects its temporal profile, correspondingly.

It is to be stressed out that as a by-product, the process potentially involves excitation of nonlinear phase via SPM, adding some B-integral as well as positive 2^{nd}-order dispersion to the pulse phase. This implies that in case obtaining the shortest available pulse from the setup is mandatory, some extra dispersion compensation may be required.

The numerical model's concept maintains two assumptions. Firstly, the KL induced within a relatively thin dielectric ("thin" refers here to negligible beam diameter variations while traversing through the dielectric), that is, the beam only obtains local angular bend and starts to converge. Naturally, the physical process involves combination of angular change and some diameter change. The propagation stage where the waist is formatted occurs outside the sample, (i.e. air or vacuum). As a byproduct, there is a lower risk of further nonlinearities accumulation, or material breakdown (air ionization starts at I$>$ 10^{13} W/cm^2). Secondly, the instantaneous nature of the nonlinear susceptibility in the dielectric, typically having a sub-femtosecond (fs) delayed response[24], enables pulses that span around multi-10s fs to ps time to experience instantaneous spatial variations and thereby contrast cleaning regardless of preceding pulse parts. Assuming sufficient pulse intensity is available, the underlying mechanism can be described as follows. Initially, low-intensity pulse parts that are temporally far from the main peak, nearly maintain their spatial properties as they merely experience any Kerr non-linearity. As a result, the beam divergence remains practically unchanged when passing the dielectric. On the contrary, higher-intensity parts, including the main peak, maintain enough energy to excite KL, which in turn modifies the beam's angular propagation, and consequently, diameter. The process is to be kept under gentle control, i.e. such that it is far enough from initiating aggressive focusing and material breakdown. Next, a spatial filter is applied such as e.g. iris / hard aperture, to filter a portion of the Gaussian beam's exterior, as shown in Fig 1.

On the downside, one can list the inevitable addition of B-integral to the pulse phase, potentially adding some temporal phase structure, that temporally broadens the incident pulse by slight up-chirp. The nonlinear B-integral phase addition can be readily estimated via[25]: $B = k_0 \cdot n_2 \int I(z)dz$, with $k_0 = 2\pi/\lambda_0$, accumulated along the pulse propagation

https://doi.org/10.1017/hpl.2023.99 Published online by Cambridge University Press

axis inside the dielectric. Some compensation to the B-integral issue can be realized by applying, e.g. controlled pulse shaping techniques[26].
It is again pointed out that the assumed applied power level does not lead to total beam collapse and optics damage. Practically this can be handled by avoiding two distinct criteria: intensities of I $\geq 10^{14}\ W/cm^2$ and fluences of $\geq 2\ J/cm^2$ for sub ps pulses[27].
As a last remark, it is reasonable to argue that the suggested method has several potential distinct benefits over well-known methods due to its ease of implementation, very low-cost components, and lack of the requirement of temporally and spatially synchronizing the beams.

3. System schematics

The experimental scheme that exploits the temporal-spatial pulse coupling is presented in Fig. 2.

We assume a collimated near-infra-red ultrashort pulse with available peak power significantly beyond the dielectric's nonlinear critical power. In the first stage, the beam is focused by a lens with a (linear) focal length f_L. For beam with a divergence angle θ (before the lens), the 4σ waist (after the lens) is: $2w_0 \approx f_L \cdot \theta$, assuming small angles approximation.

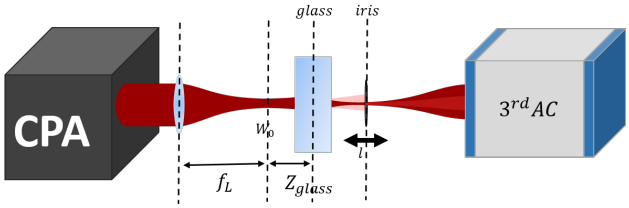

Figure 2. System schematics. f_L: linear focal lens, w_0: beam waist after the lens, z_{glass}: glass distance from w_0, l: iris-to-glass distance (movable), 3^{rd} AC: Third-order scanning autocorrelator.

Focusing the beam in the first stage is needed for initiating the nonlinear mechanism, especially in the case of fairly low pulse energies. Furthermore, as shown below, z_{glass} the glass distance from the waist is an additional tuning knob for the intensity that provided by delicately moving the glass along the beam.

Next, while the beam enters the nonlinear medium, new converging beam trajectory is induced by the Kerr effect, whose focal length can be calculated (assuming Gaussian intensity shape) by the following equation[28]:

$$f_{NL}^{-1} = \frac{8n_2 d}{\pi w^4} P \tag{1}$$

where n_2 is the nonlinear refractive index, d is the glass thickness, w is the beam radius, and P is the instantaneous laser power. Moving the glass piece with respect to the beam waist position (z_{glass}), raises several scenarios that can be roughly divided into the following categories, depending on the generated nonlinear focal length f_{NL}:

(1) The nonlinear dielectric is located at $z_{glass} = f_{NL}$, precisely compensate the linear lens power, yielding a collimated beam (Fig. 3 (a));
(2) The nonlinear dielectric is located at $z_{glass} < f_{NL}$, not compensating the linear lens and leading to a diverging beam (Fig. 3 (b));
(3) The nonlinear dielectric is located at $z_{glass} > f_{NL}$, refocusing and generating a new (nonlinear) beam waist (Fig. 3 (c));.

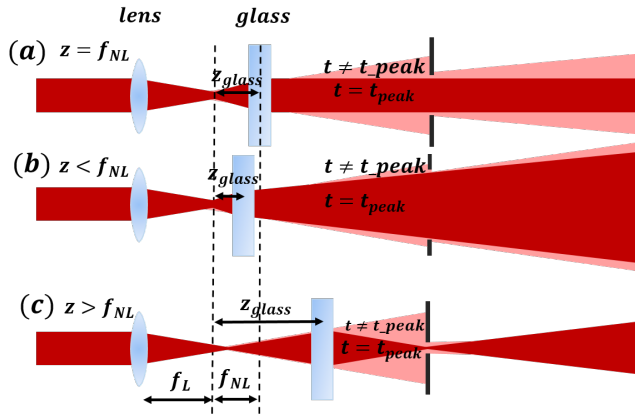

Figure 3. Illustration of the three KL focusing scenarios, obtained by varying the dielectric location with respect to the beam waist: (a) $z_{glass} = f_{NL}$, (b) $z_{glass} < f_{NL}$, and (c) $z_{glass} > f_{NL}$. Where f_L: linear lens focal length and f_{NL}: NL lens focal length. The dark red part represents the peak of the pulse where most of the NL process occurs, whereas the light red part represents lower powers and noises adjacent to the peak with weaker effect.
A crucial parameter that is, to our approach, used as a metric for the contrast change, is the peak - to - noise areas ratio at the hard aperture filtration plane. This metric shall be an estimate to the filtering ratio which finally be related to CE.

The temporal cleaning method provided in this study is based on spatial separation, practically achieved via the presence of an aperture. Looking at the three scenarios illustrated in Fig. 3, it is argued that the highest area ratio between peak (dark red) and noise (light red) is obtained in case (C), and at the tightest non-linear focus. The area ratio is as follow:

$$\frac{A'_{peak}}{A'_{noise}} = \frac{C^2 + 2C^2\frac{l(N-1)}{z_{glass}} + C^2\frac{l^2(N-1)^2}{z_{glass}^2}}{C^2 + (l + z_{glass})^2} + \tag{2}$$

$$+\frac{z_{glass}^2 + 2lNz_{glass} + l^2N^2}{C^2 + (l + z_{glass})^2}$$

Where $A = \pi w^2$, $C = \pi w_0^2/\lambda$, and l is the iris distance from the glass. N is defined here as: $N = 1 - z_{glass}/f_{NL}$. Note that $N = 0$, $N > 0$ and $N < 0$ refers to cases (a),

https://doi.org/10.1017/hpl.2023.99 Published online by Cambridge University Press

(b), and (c) respectively. The full calculation is detailed in appendix A.

As obtained from Fig. 4, for a given C (10.7 mm) and z_{glass} (6.3 mm) (according to system parameters provided at Sec. 4) and various l, the ratio of A'_{peak}/A'_{noise} has a minimum. When traveling long distances (l of $\sim$ meters scale), these minima are found around $N = 0$, i.e. $\Rightarrow f_{NL} = z_{glass}$, corresponding to case (a), whereas if traveling small distances (l of a few millimeters scale), minima are found around $N < 0$, i.e. $\Rightarrow f_{NL} < z_{glass}$, that corresponds to case (c). Additionally, for shorter iris-glass distances (l), the areas-ratio minima values (the local dips in Fig. 4) further reduces with lower N values, i.e., pointing on potentially valuable CE trend. By setting the expressions of the latter cases, one can claim that the $f_{NL} < z_{glass}$ case is optimal for discriminating between A'_{peak} and A'_{noise}, and therefore the potential for CE, is reinforced. It is therefore that in this work the most appealing approach to expect CE is under the conditions of case (c), which indeed was selected.

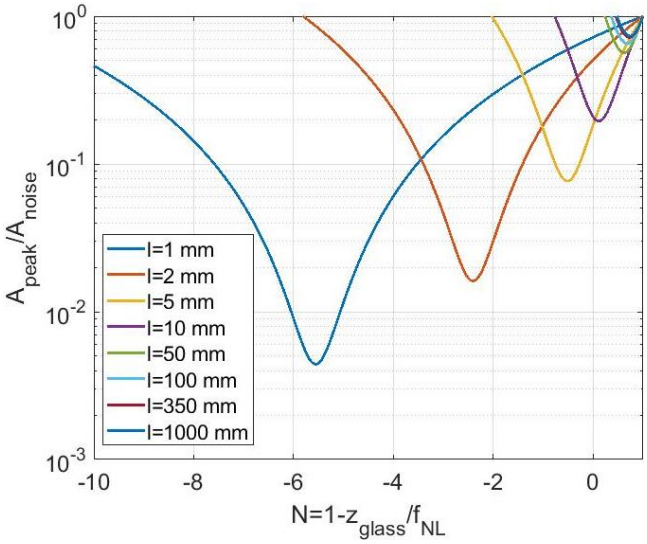

Figure 4. Peak-to-noise beam area ratios under various iris to glass distances (l) vs. N. Values of z_{glass} and C were set to 6.3 mm and 10.7 mm, respectively.

By inserting the explicit expressions: $N(z_{glass}) = 1 - z_{glass}/f_{NL}$ and $f_{NL}(z_{glass}) = B\left(1 + (z_{glass}/C)^2\right)^2$ where, $B = (\pi w_0^4)/(8n_2 dP)$ to Eq. 2, the following expression is obtained (see Appendix. B):

$$A'_{peak}/A'_{noise} = \tag{3}$$

$$\frac{C^4 l(C^4 l - 2B(C^2 + z_{glass}^2)(C^2 + z_{glass}(l + z_{glass})))}{B^2(C^2 + z_{glass}^2)^3(C^2 + (l + z_{glass})^2)} + 1$$

Obviously, one may seek for a case where the smallest A'_{peak}/A'_{noise} ratio as function of glass-iris distance (l), as well as nonlinear medium (glass) position (z_{glass}) can be obtained. A plot of Eq. 3 is shown in Fig. 5 via a 2D representation.

In addition, the location of the newly formed waist at the pulse peak ($z_{w_{0,NL}}$) can be expressed as follows (further details in Appendix. B):

$$z_{w_{0,NL}} = \frac{z_{glass} - f_{NL}}{(1 - z_{glass}/f_{NL})^2 + \left(\frac{2C}{\pi f_{NL}}\right)^2} + f_{NL} \tag{4}$$

The expression in Eq. 4 is represented by the white dashed curve in Fig. 5. It can be seen that the white line is located exactly on the minimum of A'_{peak}/A'_{noise} approving the basic estimation provided above, that the iris optimal location is at the NL peak waist location $z_{w_{0,NL}}$.

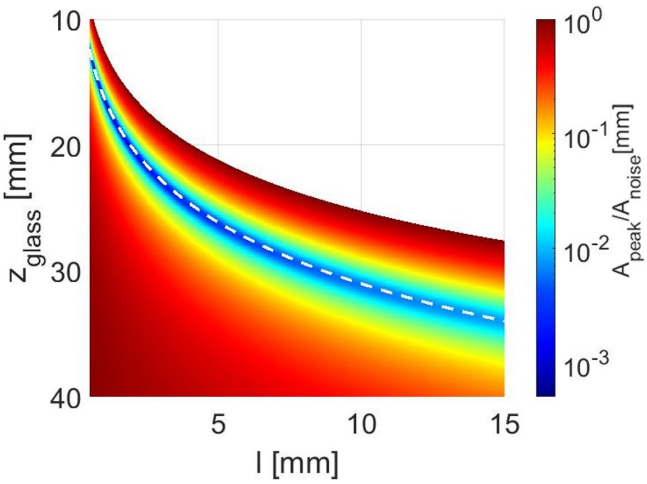

Figure 5. Two dimensional plot, showing peak-to-noise area ratio vs. l and z_{glass}. White dashed curve: $l = z_{w_{0,NL}}$

It is since that latter outcome, that the hard aperture iris was selected to be positioned at the very spot where KL-induced waist position occur: $l = z_{w_{0,NL}}$.

We would like to draw ones attention that in order to apply the model's initial assumption for thin glasses, $z_{w_{0,NL}}$ must have a lower boundary with respect to the glass thickness d . Assuming up to 10% beam diameter narrowing from the initial value, running a beam propagation code that tracks the spatial pulse dynamics [29] the aforementioned requirement is satisfied under the limit (see Appendix. C) :

$$z_{w_{0,NL}} > d/2$$

Thus, this limit is used in what follows according to the presented model.

In another aspect, the iris aperture size constitutes a trade-off between efficiency and CE, since larger aperture transmits more energy whereas a smaller aperture increases CE.

At low intensities, the iris blocks the majority of the emerging beam as its diameter (and area) is smaller relative to the pulse beam area at this position. On the contrary, near

https://doi.org/10.1017/hpl.2023.99 Published online by Cambridge University Press

the intensity peak, majority of the beam energy is confined to the nonlinear waist w_{NL}, efficiently traverses the iris, i.e. experiencing minimal attenuation.

4. Numerical model

In this section, a numerical model with parameters resembling those of the available laser system was established to evaluate the expected CE.

A temporal and spatial Gaussian shapes were assumed. Next, some temporal noise features were artificially added to the pulse vicinity, in order to represent non-ideal contrast. Noise levels are specified below. The time profile included: firstly, a sharp peak of some 100s fs duration that is typical to Yb doped glass amplifiers, accompanied by a time-exponential coherent pedestal (CP) that is typically reported to surround the peak vicinity by several 10 ps. While presented on a power scale, the CP has a linear skirt-like shape (Fig. 6). A lower noise pedestal was also introduced to represent the longer-term amplified spontaneous emission (ASE) noise in the amplifiers. This noise level typically spans multi hundreds of ps from both sides of the peak.

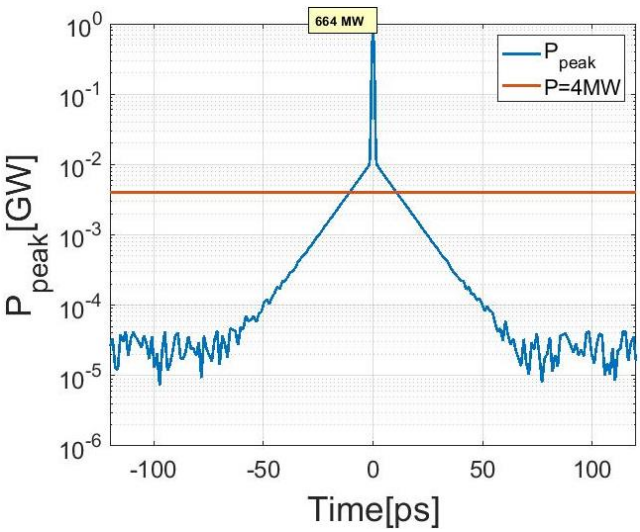

Figure 6. Pulse power vs. time. Blue: Numerically produced contrast trace of power vs. time, on a normalized power scale. Orange: A reference 4 MW power level.

In recent decade, studies pointed out that CP is attributed mainly to grating irregularities and scattering found e.g. on the groove edges [30], as well as imperfections in the (whole) stretcher and compressor structures.

Based on reports [31,32] and experience with CPA lasers, the CP and ASE were chosen in our model to have a levels of -25 and -50 dB relative to the pulse peak.

The parameters that were used in the numerical model are as follows: pulse energy E=1 mJ, central wavelength CWL=1053 nm, divergence angle θ=2 milli-Radian (mrad), and a time duration of 450 fs FWHM. The numerical temporal pulse shape is presented on a power scale in Fig. 6. In our example case, the power at the pulse's peak is $\sim$ 0.664 GW after being adjusted to the chosen energy such that $\int P(t)dt = E$, where $P(t)$ and E are power and total pulse energy.

In order to determine the appropriate z_{glass}, f_{NL} as a function of z_{glass} was calculated, based on Eq. 1. Beam waist at the glass position was derived from:

$$w(z) = w_0 \sqrt{1 + (\frac{\lambda \cdot z}{\pi \cdot w_0^2})^2}$$

where,

$$w_0 \simeq \frac{1}{2} \cdot \theta \cdot f_L$$

while P was assumed to be the pulse peak power.

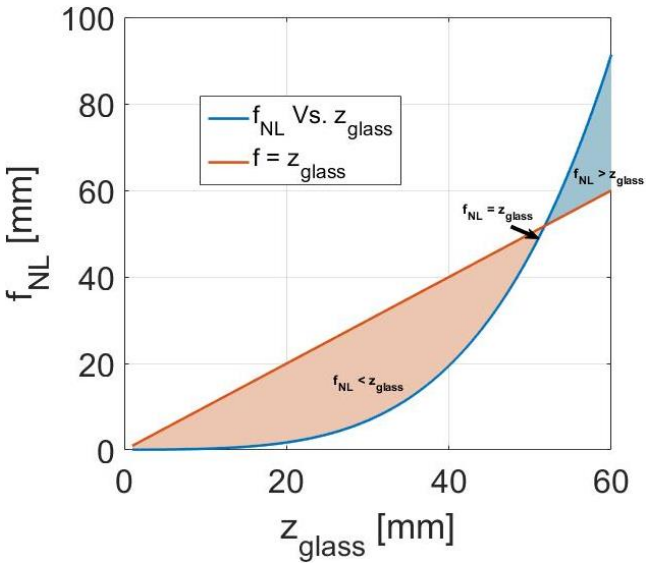

Figure 7. Kerr focal length as a function of glass distance from the beam waist position (blue), crossed with the linear $f = z_{glass}$ plot (orange). The intersection point of the two plots represents the precisely collimated case.

The resulted NL focal length as a function of z_{glass} is represented by the blue curve in Fig. 7. In order to visualize the three different cases discussed above, $f = z_{glass}$ was plotted in Fig. 7 (orange curve). According to Fig. 7, z_{glass} has to fall within the range of 0 and 52 mm in order to preserve the condition $f_{NL} < z_{glass}$. The simulation's input parameters were: $f_L = 60$ mm, d=1 mm, $\theta = 2$ mrad, $n_2 = 2.6 \cdot 10^{-20}\ m^2/W$ (typical to fused silica around 1 μm).

To obtain optimal beam areas ratio, it is beneficial to follow the A'_{peak}/A'_{noise} curve ($l = z_{w_{0,NL}}$, z_{glass}) and seek for a minimum, according to Eq. 3 at $l = z_{w_{0,NL}}$ (Eq. 4). As presented in Fig. 8, z_{glass} was chosen to be 6.3 mm.

Since in real scenarios it is not always possible to work at extremely short distances, or extremely small apertures,

https://doi.org/10.1017/hpl.2023.99 Published online by Cambridge University Press

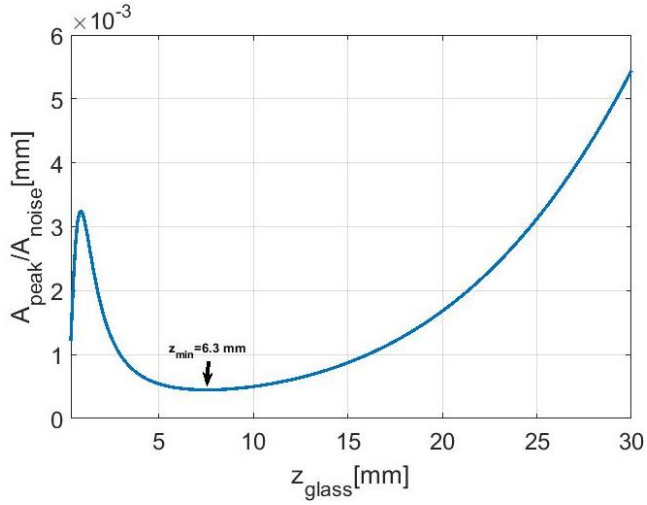

Figure 8. Beam areas peak-to-noise ratio A'_{peak}/A'_{noise} at $l = z_{w_{0,NL}}$, where minimum ratio obtained at z_{glass}=6.3 mm.

slightly larger z can be chosen in order to shift the NL focal position, or enlarge the NL focal size.

In what follows, calculation of the nonlinear focal length vs. time are provided, where Eq. 1 is applied with the optimal z_{glass} (6.3 mm). It can be inferred from Fig. 9 that f_{NL} varies from sub 0.5 mm at the pulse's peak, which indicates an extremely intense effect, to approximately a meter, when the laser power reduces below P_{cr}. Farther out, at tens of ps, f_{NL} extends to much larger values, practically implying negligible effect.

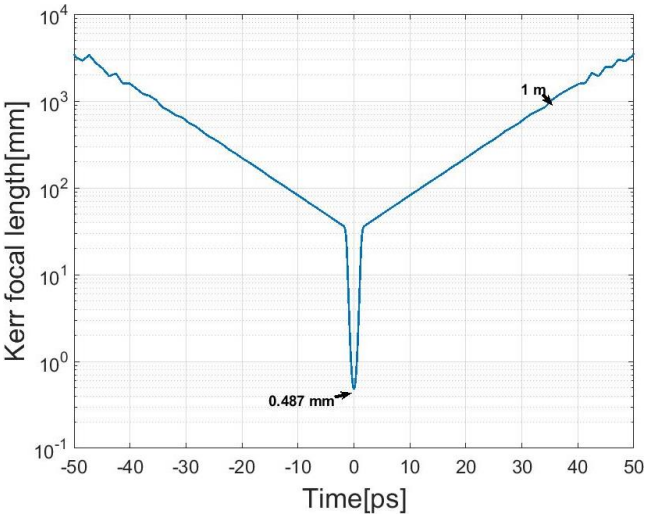

Figure 9. Kerr focal length as a function of time, based on the numerical pulse from Fig. 6 (blue).

In order to estimate the spatial filtration effect, the NL beam waist diameter was calculated, as well as the nonlinear-induced waist position (with respect to the nonlinear dielectric), according to Gaussian beam propagation equations [33]:

$$z_{0_{NL}(t)} = \left(\left(\frac{w_{0_{NL}(t)}}{w_0}\right)^2 \cdot (|z| - f_{NL}(t))\right) + f_{NL}(t) \quad (5)$$

where the nonlinear waist $w_{0_{NL}}$ is obtained by:

$$w_{0_{NL}(t)} = \frac{w_0}{\sqrt{\left(1 - \frac{z}{f_{NL}(t)}\right)^2 + \left(\frac{z_0}{f_{NL}(t)}\right)^2}} \quad (6)$$

and $z_0 = \pi w_0^2/\lambda$ is the Rayleigh length produced by the linear lens.

The calculated position of the new waist at the peak (t=0) was $z_{w_{0,NL}}(t = 0) = 0.5$ mm for the resulted f_{NL} mentioned above. It is noted that the waist position turned out to be slightly larger ($f_{NL} \sim 0.48$ mm), as a result of the preceding divergence. To obtain the strongest nonlinear gating discrimination (for the specific chosen parameters) as explained in the preceding section, the position of the hard aperture filtering was set to be $z_{w_{0,NL}}(t = 0)$.

Next, the instantaneous beam radii, obtained at the iris plane, were calculated using the following equation:

$$w(z = z_{w_{0,NL}} - z_{w_{0,NL}}(t = 0), t) = \quad (7)$$

$$w_{0_{NL}}(t)\sqrt{1 + \left(\frac{z_{w_{0,NL}}(t) - z_{w_{0,NL}}(t = 0)}{z_{0_{NL}}(t)}\right)^2}$$

where z was selected to be the distance between the iris plane ($z_{w_{0,NL}}(t = 0)$) to the time-dependent NL beam waist, and $z_{0_{NL}}$ is the NL Rayleigh length induced by that same Kerr effect.

Following the calculated waists $w_{0_{NL}}$, a two-dimensional spatial-temporal Gaussian beam shape was generated. The spatial part can be described as follows:

$$I(x, y) = I_{0,0}(t)e^{(-2\cdot(x^2+y^2)/w(z_{w_{0,NL}}(t=0),t)^2)} \quad (8)$$

where I(t) is the time pulse intensity.

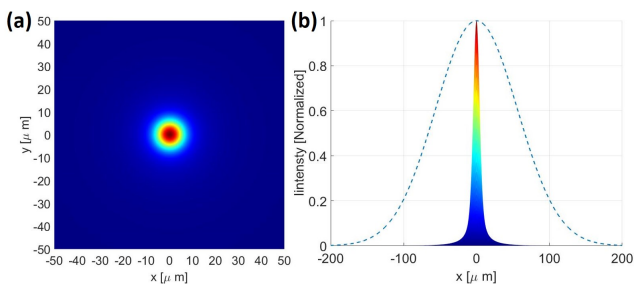

Figure 10. Sum of the 2D generated Gaussians at the iris plane in top (a) and side view (b). Dashed curve represent the normalized pulse shape assuming no NL effect.

https://doi.org/10.1017/hpl.2023.99 Published online by Cambridge University Press

The sum of all time frames at the iris plane is represented in Fig. 10. As can be seen, the final shape resembles a Gaussian, albeit with a somewhat sharper center.

In order to simulate the hard aperture spatial effect, a 2D circle with varying radii was (numerically) spatially multiplied by the 2D beam shape, in different pulse times. Fig. 11 represents this projection on x axis in different times (colorful plots), while the iris itself is represented by the black rectangle. As can be observed, the spatial pulse generated at t=0 (Fig. 11 yellow), practically completely traverses the aperture, whereas the spatial pulse preceding the peak by t=-61.6 ps (Fig. 11 purple) or earlier suffers a considerable blocking.

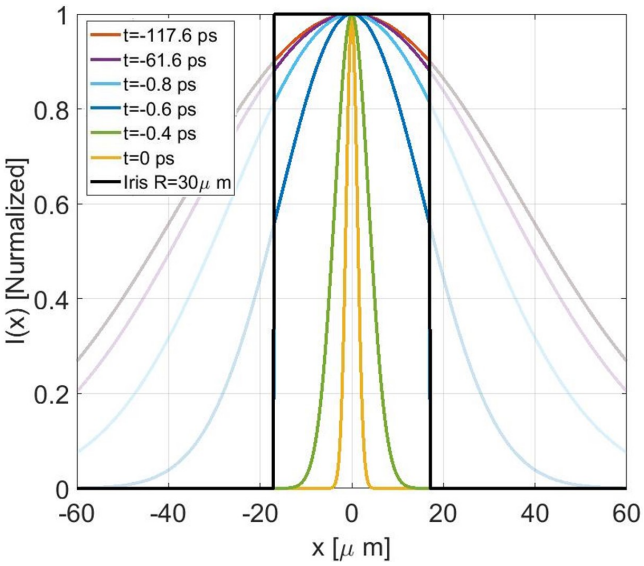

Figure 11. Spatial Gaussian pulses after experiencing the NL lens projected at the iris plane. The colored curves represent spatial pulses at various times. The (numerical) iris is represented by the black curve.

5. Results

A two stage computation was carried out in order to produce the temporal pulse profile following the spatial filtration. The iris aperture and the pulses beam shape were first spatially multiplied, and then the beam's spatial domain was integrated - $I(t) = \int\int I(x,y,t)dxdy$ to preserve only temporal dependence. Displaying the latter with unity normalization on power scale provided the temporal contrasts, for four different aperture sizes. The resultant plots are shown in Fig. 12

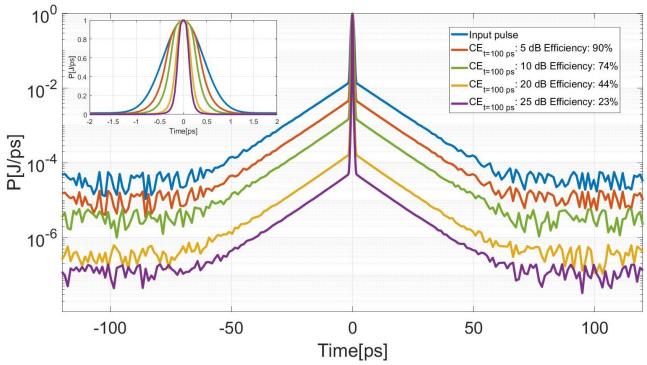

Figure 12. Contrast traces before (blue) and after KL effect and hard aperture filter, for 70 μm (orange), 34 μm (green), 10.6 μm (yellow) and 4.8 μm (purple) aperture diameters, applied upon the numeric Gaussian input beam. Inset: same plot in time scale of a few ps surrounding the peak, provided for a more detailed observation.

In addition, in order to complete the performance estimation, the whole process's efficiency was calculated by extracting the ratio of the transmitted energy to the incident energy, using the following integration:

$$\eta = \frac{\int P_{clipped} dt}{\int P_{in} dt} \tag{9}$$

Where the integrals limits in the current work were taken to within the pulse FWHM.

The aforementioned integration was carried out using a variety of aperture radii, considered in ascending order, from largest to smallest, associated to highest-to-lowest transmission, correspondingly.

For aperture diameters of : 70, 34, 10.6 , and 4.8 μm, the obtained CE factors were 5, 10, 20, and 25 dB, with corresponding efficiencies of 90%, 74%, 44%, and 23% (within FWHM pulse range) (Fig. 12). Considering different energy integration criterion, e.g. 10% power drop, yields somewhat different efficiencies: 82%, 64%, 36%, and 19%, for the same iris diameters, respectively. Of cause, as application demands, various energy integration criteria can be set.

It is however stressed out that the peak vicinity has the pronounced effect on the experiment, thus longer time consideration can be of a lesser value.

It is worth mentioning that according to simulation results, it can be concluded that a need for small apertures may be impractical. A simple way around this obstacle is applying a magnification (e.g.: an imaging stage), allowing the use of larger apertures in a real experiment.

Next, an experimental setup was set in order to validate the applicability of the above model. A full description of the experimental system can be found in Sec. 3.

The laser setup parameters are as follows: A Yb-fiber CPA with a center wavelength of λ = 1.03 μm, pulse duration of $\sim$ 450 fs (FWHM), a 4σ divergence angle of θ = 2.3 mrad

https://doi.org/10.1017/hpl.2023.99 Published online by Cambridge University Press

at the output of the CPA's compressor, and controlled pulse energies of up to several 10s of μJ.
A baseline reference contrast was set as the raw unfiltered CPA pulses, needed to be compared with respect to pulses that experienced the nonlinear effect, as proposed in the model. For evaluating the results, a 3^{rd}-order scanning AC was used (Ultrafast-Innovations "Tundra") with optical hardware dedicated to the 1 μm vicinity[34]).

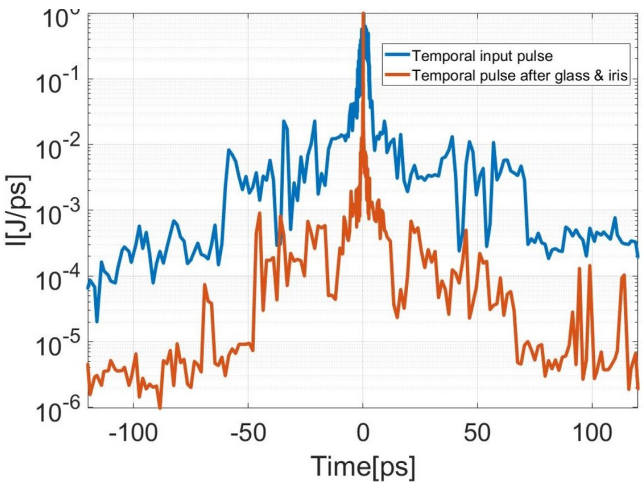

Figure 13. Measured pulse contrast before (blue) and after the KL effect and the clipping aperture (orange).

According to the experimental result that are plotted in Fig. 13, the original laser pulses yielded contrast values of around 10^4 with respect to the noise level, when observed $\pm$ 100 ps farther away of the peak, which is very typical to Yb fiber CPA laser systems. Further details of the scheme are provided in the following text. The linear lens's focal length f_L was selected to be 100 mm and the NL dielectric piece was a 0.25 inch of uncoated fused silica. The output pulse measured after the KL and a 400 μm iris aperture is represented by the orange curve in Fig. 13. Where laser input energy E=10.5 μJ, glass location Z_{glass}=3 mm, and iris location l = 7 mm. As shown, the pulse contrast was increased by nearly two orders of magnitude to $\sim 10^{-6}$, while the measured efficiency (estimated via average power) was 40% using uncoated glass (additional 8% efficiency can be excepted).
As for the nonlinear phase induced by the setup, the given parameters yield $\sim$1 Radians, which hardly disrupt the time pulse shape, and therefore its contrast as well.

It should be noted that in the experiment, lower pulse energies, and therefore, thicker glasses were applied, with refer to the model's example. It is to be stressed out that at this early stage of the study, the model refers to a simplified mechanism, in which intra-glass beam variation were negligible. In a succeeding work, a more mature model shall cover more complexities, including the processes accumulated within the glass. Such progress shall enable to validate the experiment more accurately. Additionally, energy upgrade of the scheme shall enable to operate with thinner glasses and meet cases more overlapping with the numerical model.

6. Conclusions

To conclude, a cost effective concept for CE, based on KL is proposed. Its attractiveness is based mainly on its simplicity and small number of components, basically nonlinear glass piece followed by a hard aperture. By correctly placing the components in accordance with specific pulse parameters the effect can be enhanced. An underlying theoretical and numerical descriptions was provided and expressed via formulas, and a numerical support. The method is based on the temporal dependence of the nonlinear effect. This dependence is transformed into spatial one, which is manifested back to provide the cleaner time profile. While a new spatial beam waist is created at the time-peak of the pulse (under certain conditions of $z < f_{NL}$), the weaker and noisy parts, farther from it, hardly induces any spatial changes. Therefore, while the peak traverses the aperture almost entirely, the noise (weaker) part experiences strong losses, resulting in an overall CE. The current numerical model works as follows: it translated the instantaneous pulse's intensity into 2-D spatial beam distribution variations, followed by 2-D multiplication by a hard clip circular aperture. Finally, data is returned to the time domain by spatial integration. In comparison to other CE techniques (e.g., OPA, XPW act.), one can realize the attractiveness of the proposed approach, considering the overall combination of CE degree, efficiency, and low cost. The model predicts typical efficiencies that vary between, e.g., 90%, for 5 dB CE, to 23% for 25 dB CE. In addition, we conducted an experiment that confirmed the numerical result, and demonstrated two orders of magnitude CE at expense of 40% efficiency. As a final remark, it is further stressed out that the technique is simple to implement, not requiring beam synchronization or exotic materials. Therefore laser labs can consider to benefit from CE upgrade with good efficiency, that is to operate high energy CPA systems with better performance. Further planned studies are underway, one aims at expanding the numerical model to cover thick glasses and another at empirically testing the model under higher energies and different glass thicknesses.

A. Beam area calculation for pulse peak vs. noise for the 3 cases

A calculation for the beam area, assuming the formation of a nonlinear lens in the glass - f_{NL} at the pulse's peak is presented below.

https://doi.org/10.1017/hpl.2023.99 Published online by Cambridge University Press

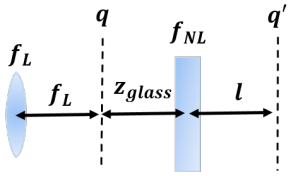

Figure 14. Diagram description of the system precisely at the pulse peak time point, when a non-linear lens with a focal length f_{NL} is produces. f_L: linear focal length (converging lens), z_{glass}: glass distance from beam waist (w_0), l : distance from the glass where the area ratio was evaluated (also, is the iris aperture location).

A Gaussian beam can be described by a complex parameter q, which contains information both on beam radius w and wave-front radius of curvature R [35]:

$$\frac{1}{q} = -i\frac{\lambda}{\pi w^2} + \frac{1}{R}$$

As can be seen in Fig. 14, q is taken to be at the linear lens focal plane f_L, hence, $R \Rightarrow \infty$ and $w = w_0$:

$$\Longrightarrow q = i\frac{\pi w_0^2}{\lambda} = iC$$

It is now possible to apply the ABCD matrix technique for evaluating the pulse peak spatial propagation in the NL process.

$$\begin{pmatrix} A_{peak} & B_{peak} \\ C_{peak} & D_{peak} \end{pmatrix} = \begin{pmatrix} 1 & l \\ 0 & 1 \end{pmatrix} \cdot \begin{pmatrix} 1 & 0 \\ -1/f_{NL} & 1 \end{pmatrix} \cdot \begin{pmatrix} 1 & z_{glass} \\ 0 & 1 \end{pmatrix}$$

That is:

$$\begin{pmatrix} A_{peak} & B_{peak} \\ C_{peak} & D_{peak} \end{pmatrix} = \begin{pmatrix} 1 - l/f_{NL} & z_{glass} + l - z_{glass}l/f_{NL} \\ -1/f_{NL} & 1 - z_{glass}/f_{NL} \end{pmatrix}$$

Let us define a variable: $N = 1 - z_{glass}/f_{NL}$, [$\Rightarrow 1/f_{NL} = (1-N)/z_{glass}$]: according to which, negative N values expresses $z_{glass} > f_{NL}$ (case (c) at Sec. 3), and vice versa. Further developing the latter yields the following,

$$\begin{pmatrix} A_{peak} & B_{peak} \\ C_{peak} & D_{peak} \end{pmatrix} = \begin{pmatrix} 1 + \frac{l(N-1)}{z_{glass}} & z_{glass} + lN \\ \frac{N-1}{z_{glass}} & N \end{pmatrix}$$

$$q'_{peak} = \frac{A_{peak}q + B_{peak}}{C_{peak}q + D_{peak}}$$

where q' represent the Gaussian beam at the iris location as can be observed in Fig. 14. By definition:

$$\frac{1}{q'_{peak}} = -i\frac{\lambda}{\pi w'^2_{peak}} + \frac{1}{R'_{peak}}$$

The following can be inferred:

$$\Rightarrow A_{peak} = -\frac{\lambda}{Im\left(1/q'_{peak}\right)}$$

where $A'_{peak} = \pi {w'_{peak}}^2$.

$$\frac{1}{q'_{peak}} = \frac{C_{peak}q + D_{peak}}{A_{peak}q + B_{peak}}$$

Comparing only the imaginary parts:

$$Im\left(\frac{1}{q'_{peak}}\right) = Im\left(\frac{C_{peak}q + D_{peak}}{A_{peak}q + B_{peak}}\right) =$$

$$= Im\left(\frac{C_{peak}iC + D_{peak}}{A_{peak}iC + B_{peak}}\right) =$$

$$= Im\left(\frac{(C_{peak}iC + D_{peak})(-A_{peak}iC + B_{peak})}{(A_{peak}iC + B_{peak})(-A_{peak}iC + B_{peak})}\right)$$

$$= Im\left(\frac{C_{peak}A_{peak}C^2 - iCD_{peak}A_{peak}}{A^2_{peak}C^2 + B^2_{peak}}\right) +$$

$$Im\left(\frac{iCC_{peak}B_{peak} + D_{peak}B_{peak}}{A^2_{peak}C^2 + B^2_{peak}}\right) =$$

$$= C\frac{C_{peak}B_{peak} - D_{peak}A_{peak}}{A^2_{peak}C^2 + B^2_{peak}}$$

Therefore,

$$A'_{peak} = -\frac{\lambda}{C}\frac{A^2_{peak}C^2 + B^2_{peak}}{C_{peak}B_{peak} - D_{peak}A_{peak}} =$$

$$-\frac{\lambda}{C}\frac{(1 + \frac{l(N-1)}{z_{glass}})^2C^2 + (z_{glass} + lN)^2}{(\frac{N-1}{z_{glass}})(z_{glass} + lN) - N(1 + \frac{l(N-1)}{z_{glass}})} \Rightarrow$$

$$A'_{peak} = \lambda C + 2\lambda C\frac{l(N-1)}{z_{glass}} + \lambda C\frac{l^2(N-1)^2}{z^2_{glass}} +$$

$$+\frac{\lambda}{C}z^2_{glass} + 2lN\frac{\lambda}{C}z_{glass} + \frac{\lambda}{C}l^2N^2$$

In addition, a computation of the beam area farther from the pulse vicinity (noise) is shown below, assuming no nonlinear lensing occur within the glass.

https://doi.org/10.1017/hpl.2023.99 Published online by Cambridge University Press

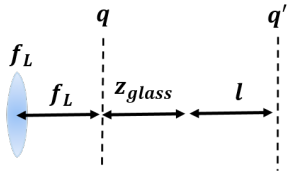

Figure 15. System diagram describing the low pulse intensities and noise, where one assumes no generation of a non-linear lens f_{NL} in the glass. f_L: linear focal length, z_{glass}: glass distance from beam waist (w_0), l : distance from the glass where the areas ratio was evaluated (also is the aperture position).

$$\begin{pmatrix} A_{noise} & B_{noise} \\ C_{noise} & D_{noise} \end{pmatrix} = \begin{pmatrix} 1 & l \\ 0 & 1 \end{pmatrix} \cdot \begin{pmatrix} 1 & z_{glass} \\ 0 & 1 \end{pmatrix} = \begin{pmatrix} 1 & l + z_{glass} \\ 0 & 1 \end{pmatrix} \Rightarrow$$

Therefore, since $q = iC$ as mentioned above:

$$q'_{noise} = \frac{A_{noise}q + B_{noise}}{C_{noise}q + D_{noise}} = iC + l + z_{glass}$$

$$A'_{noise} = \pi w'^2_{noise} = -\lambda \cdot Im^{-1}(1/q'_{noise}) =$$

$$= -\lambda \cdot Im^{-1}\left(1/(iC + l + z_{glass})\right) = \frac{\lambda}{C}(C^2 + (l + z_{glass})^2)$$

Resulting in:

$$\Rightarrow \frac{A'_{peak}}{A'_{noise}} = \frac{C^2 + 2C^2\frac{l(N-1)}{z_{glass}} + C^2\frac{l^2(N-1)^2}{z^2_{glass}}}{C^2 + (l + z_{glass})^2} + \quad (10)$$

$$\frac{z^2_{glass} + 2lNz_{glass} + l^2N^2}{C^2 + (l + z_{glass})^2}$$

B. Beam area calculation for pulse peak vs. noise as a function of the glass and iris positions

Here an optimal iris position (l) and glass position (z_{glass}) are calculated, according to the peak-to-noise beam areas ratio (expressions were obtained in Appendix A). Inserting $N = 1 - f_{NL}/z_{glass}$ to A'_{peak}/A'_{noise} from Eq. 10, Appendix A:

$$\frac{A'_{peak}}{A'_{noise}} = \frac{\frac{C^2l^2}{f^2_{NL}} - \frac{2C^2l}{f_{NL}} + C^2 + l^2(1 - \frac{z_{glass}}{f_{NL}})^2}{C^2 + (l + z_{glass})^2} +$$

$$\frac{2lz(1 - \frac{z_{glass}}{f_{NL}}) + z^2_{glass}}{C^2 + (l + z_{glass})^2}$$

In addition, f_{NL} depends on z, according to the next equation:

$$\frac{1}{f_{NL}} = \frac{8n_2d}{\pi w^4}P \Rightarrow$$

$$f_{NL} = \frac{\pi}{8n_2dP}\left(w_0\sqrt{1 + \left(\frac{\lambda z_{glass}}{\pi w_0^2}\right)^2}\right)^4 =$$

$$= \frac{\pi w_0^4}{8n_2dP}\left(1 + \left(\frac{z_{glass}}{C}\right)^2\right)^2 = B\left(1 + \left(\frac{z_{glass}}{C}\right)^2\right)^2$$

where $B = \frac{\pi w_0^4}{8n_2dP}$.

$$\Rightarrow A'_{peak}/A'_{noise}(z_{glass}, l) = \quad (11)$$

$$\frac{C^4l(C^4l - 2B(C^2 + z^2_{glass})(C^2 + z_{glass}(l + z_{glass})))}{B^2(C^2 + z^2_{glass})^3(C^2 + (l + z_{glass})^2)} + 1$$

Moreover, the location of the new waist is:

$$z_{w_{0,NL}} = (z_{glass} - f_{NL})\left(\frac{w_{0_{NL}}}{w_0}\right)^2 + f_{NL}$$

where:

$$w_{0_{NL}} = \frac{w_0}{\sqrt{(1 - z_{glass}/f_{NL})^2 + \left(\frac{2w_0^2}{\lambda f_{NL}}\right)^2}}$$

$$\Rightarrow z_{w_{0,NL}} = \frac{z_{glass} - f_{NL}}{(1 - z_{glass}/f_{NL})^2 + \left(\frac{2C}{\pi f_{NL}}\right)^2} + f_{NL}$$

The optimal iris position was obtained based on the schematic shown in Fig. 5, Sec. 3. The value $z_{w_{0,NL}}$ results in the minimal areas-ratio obtained in Eq. 11. By inserting $l = z_{w_{0,NL}}$ into Eq. 11 one can obtain the optimal z_{glass} by finding the minimal area ratio. This can be done either by plotting it as function of z_{glass} (Fig . 8), or by taking its derivative expression and setting to 0.

https://doi.org/10.1017/hpl.2023.99 Published online by Cambridge University Press

C. Beam waist propagation inside the glass

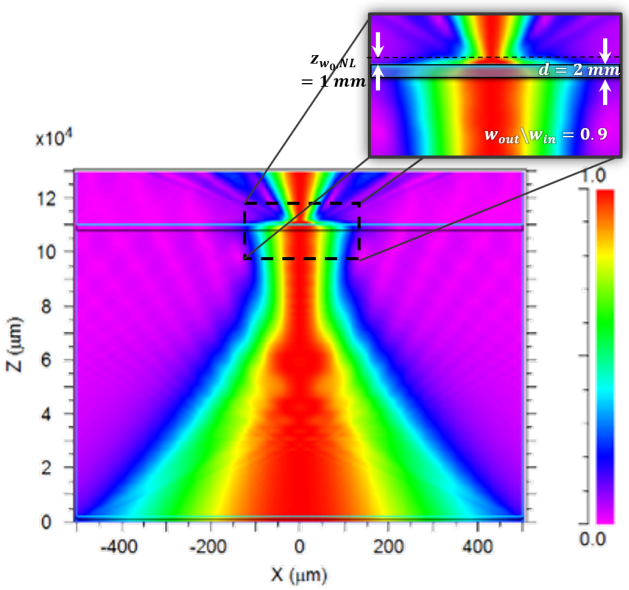

Figure 16. Beam propagation simulation showing spatial pulse variations. Starting from bottom: beam convergence is observed after leaving the linear lens. "Linear" waist is seen where the narrowest diameter is obtained ($\sim$ upper $\frac{2}{3}$ of the figure). Nonlinear dielectric is sketched in a cyan line. Major convergence occur after leaving the nonlinear sample, in air. The nonlinear waist is seen as the narrowest beam near the end (top)

In order to determine the shortest limit for $z_{w_0,NL}$ where thin glass approximation is valid, a beam propagation method simulation [29] was used. The parameters that were considered were in consistence with the numerical simulation parameters presented in Sec. 4.

As obtained from Fig. 16 the beam diameter drops by 90% in the case were the glass thickness (d) is double the new formatted NL waist ($z_{w_0,NL}$): d=2 mm and $z_{w_0,NL}$=1 mm.

References

1. Maine, P., Strickland, D., Bado, P., Pessot, M., and Mourou, G., "Generation of ultrahigh peak power pulses by chirped pulse amplification", IEEE Journal of Quantum electronics, 24(2), 398-403, (1988).
2. Murnane, M. M., Kapteyn, H. C., and Falcone, R. W., "High-density plasmas produced by ultrafast laser pulses". Physical review letters, 62(2), 155, (1989).
3. Neely, D., Foster, P., Robinson, A., Lindau, F., Lundh, O., Persson, A., Wahlström, C.-G., and McKenna, P., "Enhanced proton beams from ultrathin targets driven by high contrast laser pulses". Applied Physics Letters, 89(2), (2006).
4. J. P. Singh and S. N. Thakur, "*Laser-induced breakdown spectroscopy*" (Elsevier, 2020) p.4148.
5. Sharma, P., and Vatsa, R. K., "Nanoclusters Under Extreme Ionization Conditions". In Materials Under Extreme Conditions (Elsevier, 2017) (pp. 575-613).
6. Jean-Philippe Rousseau (LOA), Rodrigo Lopez-Martens (LOA), Lourdes Patricia Ramirez (LCFIO), Dimitris N. Papadopoulos (LCFIO), Alain Pellegrina (ILE, LCFIO), Frédéric Druon (LCFIO), Patrick Georges (LCFIO) Jullien, A., Chen, X., Ricci, A., Rousseau, J. P., Lopez-Martens, R., Ramirez, L. P., Papadopoulos D. N., Pellegrina A., Druon F., and Georges, P., "High-contrast Ultrabroadband Frontend Source for High Intensity Few-Cycle Lasers". arXiv preprint arXiv:1109.1992 (2011).
7. Shen, L., Li, Y., Li, W., Song, J., Qian, J., Sun, J., Feng, R., Peng, Y., and Leng, Y., "High temporal contrast 1053 nm laser source based on optical parametric amplification and second-harmonic generation". High Power Laser Science and Engineering, 11, e1, (2023).
8. Ma, J., Yuan, P., Wang, Y., Zhu, H., and Qian, L., "Numerical study on pulse contrast enhancement in a short-pulse-pumped optical parametric amplifier". Optics Communications, 285(21-22), 4531-4536, (2012).
9. Wang, Z., Liu, C., Shen, Z., Zhang, Q., Teng, H., and Wei, Z., "High-contrast 1.16 PW Ti: sapphire laser system combined with a doubled chirped-pulse amplification scheme and a femtosecond optical-parametric amplifier", Optics letters, 36(16), 3194-3196, (2011).
10. Huang, Y., Zhang, C., Xu, Y., Li, D., Leng, Y., Li, R., and Xu, Z., "Ultrashort pulse temporal contrast enhancement based on noncollinear optical-parametric amplification", Optics letters, 36(6), 781-783, (2011).
11. Doumy, G., Quéré, F., Gobert, O., Perdrix, M., Martin, Ph., Audebert, P., Gauthier, J. C., Geindre, J. P., and Wittmann, T., "Complete characterization of a plasma mirror for the production of high-contrast ultraintense laser pulses", Physical Review E, 69(2), 026402, (2004).
12. Kalashnikov, M. P., Risse, E., Schönnagel, H., and Sandner, W., "Double chirped-pulse-amplification laser: a way to clean pulses temporally", Optics letters, 30(8), 923-925, (2005).
13. Liu, J., Okamura, K., Kida, Y., and Kobayashi, T., "Temporal contrast enhancement of femtosecond pulses by a self-diffraction process in a bulk Kerr medium", Optics Express, 18(21), 22245-22254, (2010).
14. Wang, X. Z., Wang, Z. H., Wang, Y. Y., Zhang, X., Song, J. J., and Wei, Z. Y., "A Self-Diffraction Temporal Filter for Contrast Enhancement in Femtosecond Ultra-High Intensity Laser", Chinese Physics Letters, 38(7), 074202, (2021).
15. Shen, X., Wang, P., Liu, J., and Li, R., "Linear angular dispersion compensation of cleaned self-diffraction light with a single prism", High Power Laser Science and Engineering, 6, e23, (2018).
16. Xie, N., Huang, X., Wang, X., Zhou, K., Sun, L., Guo,

https://doi.org/10.1017/hpl.2023.99 Published online by Cambridge University Press

Y., and Su, J., "Temporal contrast improvement by a self-diffraction process for a petawatt-class Ti: sapphire laser", Journal of Modern Optics, 67(15), 1314-1320, (2020).
17. Zhu, P., Zigler, A., Xie, X., Zhang, D., Yang, Q., Sun, M., Papeer, J.,Kang, J., Gao, Q., Liang, X., Zhu, H., Guo, A., Liang, Y., Ji, Sh., Ren, L., Liu, H., Kang, N.,Zhao, Y., and Zhu, J., "Temporal contrast enhancement of ultrashort pulses using a spatiotemporal plasma-lens filter", Optics letters, 45(8), 2279-2282, (2020).
18. Kelley, P. L., "Self-focusing of optical beams", Physical Review Letters, 15 (26), 1005 (1965).
19. Gaeta, A. L., "Catastrophic collapse of ultrashort pulses", Physical Review Letters, 84 (16), 3582, (2000).
20. Lariontsev, E. G., and Serkin, V. N., "Possibility of using self-focusing for increasing contrast and narrowing of ultrashort light pulses", Soviet Journal of Quantum Electronics,5 (7), 796, (1975).
21. Liu, Z., Wright, L. G., Christodoulides, D. N., and Wise, F. W., "Kerr self-cleaning of femtosecond-pulsed beams in graded-index multimode fiber", Optics letters, 41 (16), 3675-3678, (2016).
22. Shen, X., Wang, P., Zhu, J., Si, Z., Zhao, Y., Liu, J., and Li, R., "Temporal contrast reduction techniques for high dynamic-range temporal contrast measurement", Optics Express, 27 (8), 10586-10601, (2019).
23. Lu, X., and Leng, Y., "Demonstration of contrast improvement and spectral broadening in thin solid plates", Optics Letters, 46 (20), 5108-5111, (2021).
24. A. Weiner, "*Ultrafast optics*", Vol. 72 (John Wiley & Sons, 2011) p. 57.
25. Weber, M. J., Milam, D., and Smith, W. L., "Nonlinear refractive index of glasses and crystals", Optical Engineering, 17 (5), 463-469, (1978).
26. Verluise, F., Laude, V., Cheng, Z., Spielmann, C., and Tournois, P., "Amplitude and phase control of ultrashort pulses by use of an acousto-optic programmable dispersive filter: pulse compression and shaping". Optics letters, 25 (8), 575-577, (2000).
27. Bendib, A., Bendib-Kalache, K., and Deutsch, C., "Optical breakdown threshold in fused silica with femtosecond laser pulses", Laser and Particle Beams, 31 (3), 523-529, (2013).
28. Marburger, J. H., "Self-focusing: theory",Progress in quantum electronics, 4, 35-110, (1975).
29. BeamPROP, https://www.synopsys.com/photonic-solutions/rsoft-photonic-device-tools/passive-device-beamprop.html.
30. Hooker, C., Tang, Y., Chekhlov, O., Collier, J., Divall, E., Ertel, K., Hawkes, S., Parry, B., and Rajeev, P. P., "Improving coherent contrast of petawatt laser pulses", Optics express, 19 (3), 2193-2203, (2011).
31. Danson, C., Neely, D., and Hillier, D., "Pulse fidelity in ultra-high-power (petawatt class) laser systems", High Power Laser Science and Engineering, 2, e34, (2014).
32. Buldt, J., Mueller, M., Klas, R., Eidam, T., Limpert, J., and Tünnermann, A., "Enhancement of temporal contrast by filtered SPM broadened spectra", In Advanced Solid State Lasers (pp. JM5A-25). Optica Publishing Group, (2017, October).
33. Self, S. A., "Focusing of spherical Gaussian beams", Applied optics, 22 (5), 658-661, (1983).
34. Ultrafast innovations, www.ultrafast-innovations.com.
35. Bélanger, P. A., "Beam propagation and the ABCD ray matrices", Optics letters, 16 (4), 196-198, (1991).

https://doi.org/10.1017/hpl.2023.99 Published online by Cambridge University Press